









Macrophages producing chondroitin sulfate proteoglycan-4 induce neuro-cardiac junction impairment in Duchenne muscular dystrophy

Marika Milan^{1,2} , Fabio Maiullari^{2,3} , Maila Chirivì^{1,4}, Maria Grazia Ceraolo^{1,2}, Rebecca Zigiotta², Andrea Solun^{5,6} , Silvia Maiullari⁶, Elisa Landoni⁷, Dario Di Silvestre⁸, Francesca Brambilla⁸, Pierluigi Mauri⁸, Veronica De Paolis⁶ , Nicole Fratini⁴ , Maria Cristina Crosti², Chiara Cordiglieri², Chiara Parisi⁶ , Antonella Calogero⁹, Dror Seliktar¹⁰, Yvan Torrente¹, Chiara Lanzuolo^{2,8}, Gianpietro Dotti⁷, Mirco Toccafondi², Mauro Bombaci², Elena De Falco⁹, Claudia Bearzi^{2,8}  and Roberto Rizzi^{2,9*} 

¹ Neurology Unit, Fondazione IRCCS Ca' Granda Ospedale Maggiore Policlinico, Milan, Italy

² Fondazione Istituto Nazionale di Genetica Molecolare (INGM) 'Romeo ed Enrica Invernizzi', Milan, Italy

³ PhD Program in Cellular and Molecular Biology, Department of Biology, University of Rome 'Tor Vergata', Rome, Italy

⁴ Department of Molecular Medicine, Sapienza University, Rome, Italy

⁵ Unit of Molecular Neurosciences, University Campus Bio-Medico, Rome, Italy

⁶ Institute of Biochemistry and Cell Biology, National Research Council, Rome, Italy

⁷ Lineberger Comprehensive Cancer Center, University of North Carolina at Chapel Hill, Chapel Hill, NC, USA

⁸ Institute of Biomedical Technologies, National Research Council, Milan, Italy

⁹ Department of Medical-Surgical Sciences and Biotechnologies, Sapienza University of Rome, Latina, Italy

¹⁰ Department of Biomedical Engineering, Technion Institute, Haifa, Israel

*Correspondence to: R. Rizzi, Department of Medical-Surgical Sciences and Biotechnologies, Sapienza University of Rome, C.so della Repubblica, 79, 04100 Latina, Italy. E-mail: roberto.rizzi@uniroma1.it

Abstract

Duchenne muscular dystrophy (DMD) is caused by the absence of the full form of the dystrophin protein, which is essential for maintaining the structural integrity of muscle cells, including those in the heart and respiratory system. Despite progress in understanding the molecular mechanisms associated with DMD, myocardial insufficiency persists as the primary cause of mortality, and existing therapeutic strategies remain limited. This study investigates the hypothesis that a dysregulation of the biological communication between infiltrating macrophages (MPs) and neurocardiac junctions exists in dystrophic cardiac tissue. In a mouse model of DMD (*mdx*), this phenomenon is influenced by the over-release of chondroitin sulfate proteoglycan-4 (CSPG4), a key inhibitor of nerve sprouting and a modulator of the neural function, by MPs infiltrating the cardiac tissue and associated with dilated cardiomyopathy, a hallmark of DMD. Givinostat, the histone deacetylase inhibitor under current development as a clinical treatment for DMD, is effective at both restoring a physiological microenvironment at the neuro-cardiac junction and cardiac function in *mdx* mice in addition to a reduction in cardiac fibrosis, MP-mediated inflammation, and tissue CSPG4 content. This study provides novel insight into the pathophysiology of DMD in the heart, identifying potential new biological targets.

© 2024 The Author(s). *The Journal of Pathology* published by John Wiley & Sons Ltd on behalf of The Pathological Society of Great Britain and Ireland.

Keywords: cardiac innervation; dilated cardiomyopathy; DMD heart failure; macrophages; proteoglycans; extracellular matrix; inflammation; cardiac fibrosis

Received 22 February 2024; Revised 12 August 2024; Accepted 1 October 2024

No conflicts of interest were declared.

Introduction

Duchenne muscular dystrophy (DMD) is an X-linked disorder caused by mutations in the dystrophin gene, a key protein connecting the internal cytoskeleton to the extracellular matrix (ECM) [1]. Although skeletal muscle impairment is most prominent, DMD also adversely affects myocardial and nervous system function [2].

Research on DMD has advanced in managing heart dysfunction by addressing molecular imbalances in

cardiomyocytes (CMs), such as increased intracellular calcium (Ca^{2+}), dysfunctional SarcoEndoplasmic Reticulum Calcium ATPase (SERCA) activity, and elevated ROS production [3]. Despite several therapeutic approaches targeting dystrophin or utrophin transcription [4], preventing disease progression remains elusive due to poorly understood maladaptive cardiac function often attributed to excessive fibrosis.

Chronic immune system activity, particularly involving T lymphocytes and macrophages (MPs), plays a critical

role in DMD pathogenesis, with an inflammatory phenotype predominant [5]. However, the interplay between pro- (M1) and anti-inflammatory (M2) MPs generates a complex inflammatory feedback loop. Chronic activation of M1 MPs also triggers an excessive response from M2 MPs, leading to the overproduction of ECM [6,7]. This imbalance significantly contributes to cardiac fibrosis, exacerbating the loss of myocardium function [8]. Additionally, membrane instability due to Ca²⁺ dysregulation (caused by dystrophin absence) damages the cardiac muscle and induces chronic permeabilization to inflammatory infiltrate, exacerbating the massive production of extracellular fluid containing ECM from the fibrotic tissue [9]. Dysfunctional mitophagy, oxidative stress, CM death, and mechanical impairment are also described in dystrophic cardiac tissue [10].

Beyond inflammation, dystrophin serves as a crucial link between motor neurons and skeletal muscles [11]. Its absence in DMD disrupts synaptic structure and function, affecting the cyclic AMP (cAMP) compartmentalization and beta-adrenoceptors stimulation [12]. Dystrophic mice (*mdx* mice) exhibit decreased sympathetic innervation density in the heart [2].

This study proposes a novel perspective on DMD's cardiac pathology, focusing on the perturbed communication between the immune system and the neuro-cardiac junction (NCJ).

Inflammatory MP infiltrates and alterations in proteins controlling synaptic function have been observed in *mdx* mouse hearts. An excessive release of chondroitin sulfate proteoglycan-4 (CSPG4) within the infiltrate was identified. This proteoglycan, known to inhibit ocular muscle innervation and to be overexpressed during skeletal muscle regeneration in DMD patients [13], also regulates neuronal networks [14]. Co-culture experiments with chimeric antigen receptor T lymphocytes (CARTs) targeting CSPG4 demonstrate that MPs produce this proteoglycan, inhibiting axon growth in a 3D model of NCJ via a paracrine mechanism.

Considering that dilated cardiomyopathy in DMD results from tissue denervation and muscle tone loss [15], it is conceivable that cardiac function impairment might stem from the immune system altering stromal proteins controlling the communication with the NCJ. Most DMD studies focus on neuromuscular junctions, overlooking the potentially interesting link between inflammation and NCJ via ECM proteoglycans.

Understanding this interaction could reveal new therapeutic targets and intervention areas, to provide novel insights into DMD pathology and management.

Materials and methods

Ethical approval

All procedures involving living animals were performed in conformity with the experimental protocols approved by the Ministry of Health (Protocol 717/2018 and Protocol 1188/2020). All manipulations were carried out by

qualified personnel and under the guidelines from Directive 2010/63/EU of the European Parliament on the protection of animals used for scientific purposes. The methods used for euthanasia were isoflurane inhalation (1.2–2.0% in 100% oxygen) or tiletamine/zolazepam (60 mg/kg) and xylazine (5 mg/kg).

Mice and treatments

Three- and 10-month-old dystrophic (C57BL/10-*mdx*) and healthy wild type (WT) mice (C57BL/10) were used. The *mdx* mice were divided into two groups. The first group (Givinostat) received a daily i.p. injection of givinostat (Giv) dissolved in saline (5 mg/kg/day) for 60 days. The second group (control) received saline.

Cardiac characterization

Echocardiogram

Mice were anesthetized with isoflurane (1.2–2.0% in 100% oxygen) and maintained at 37 °C. Imaging was performed on days 0, 1, 3, 7, 15, 30, and 60 using VisualSonics Vevo 3100 (Fujifilm, Amsterdam, The Netherlands), as previously described [16,17].

Hemodynamic

Anesthetized mice with isoflurane inhalation. A polyethylene catheter was inserted into the right carotid artery and connected to a transducer to measure left ventricular (LV) systolic and diastolic pressure.

Histological analysis

The animals were anesthetized with tiletamine/zolazepam and xylazine. Hearts were perfused with 50 mM KCl via abdominal aortic cannulation, then excised and either embedded in Tissue-Tek O.C.T. (Catalogue No. 361603E, VWR International S.r.l, Milan, Italy) or paraffin. Hearts in O.C.T. were dipped in cold isobutane and sectioned at 8 µm using a cryostat. For paraffin sections, hearts were fixed in 10% neutral-buffered formalin, dehydrated with alcohol, embedded in paraffin, and sectioned into 2-µm slices using a microtome. Frozen heart tissues were warmed to room temperature (RT) for 20 min, fixed in ice-cold acetone for 5 min, then washed in PBS. Paraffin sections were deparaffinized in xylene and rehydrated with descending alcohols. Antigen retrieval was done using citrate buffer (0.1 M, pH 6.0). Frozen and paraffin sections were blocked for 30 min at RT with 5% bovine serum albumin (BSA, Catalogue No. A1470, Sigma-Aldrich, Saint Louis, MO, USA), incubated overnight at 4 °C with primary antibodies: anti-cardiac troponin T (cTNNT, 1:100, Abcam, ab33589, Cambridge, UK), anti-Connexin 43 (Cx43, 1:100, Cell Signaling Technology (CST), #3512, Danvers, MA, USA), anti-tyrosine hydroxylase (TH, 1:100, Sigma-Aldrich, ab152), anti-Synapsin 1 (SYN1, 1:100, CST, #6710, Danvers, MA, USA), anti-MPs F4/80 (F4/80, 1:100, Biorad, MCA497G, Segrate, Milan, Italy), anti-CSPG4 (1:200, Novus Biologicals,

NBP266979 or 1:50, Abingdon, Oxfordshire, UK, Santa Cruz, SC-80003, Dallas, TX, USA), and anti-fibronectin 1 (FN1; 1:50, Santa Cruz, SC-271098) and incubated with fluorescent-conjugated secondary antibodies (1:1000, Invitrogen, Waltham, MA, USA) for 1 h. Nuclei were counterstained with DAPI (Catalogue No. D1306, Invitrogen). Images were acquired using a confocal microscope TCS SP5 (Leica Microsystems, Wetzlar, Germany). The fibrotic index was determined using Masson's Trichrome assay (Catalogue No. AUS240, Bioptica, Milan, Italy) staining, following the manufacturer's protocol. Scar size was expressed as the ratio of the fibrotic area to the total area. CX43 quantification was performed as described previously [16]. Innervation density was evaluated using TH and SYN1 antibody staining. All images were analyzed using ImageJ [Rasband, W.S. (1997–2015) ImageJ, National Institutes of Health, Bethesda, MD, USA, <http://imagej.nih.gov/ij>].

Immunofluorescence analysis

MPs were fixed in 4% paraformaldehyde for 10 min, permeabilized with 0.1% TRITON X-100 (Sigma-Aldrich) in PBS for 10 min, and blocked in 5% BSA-PBS for 45 min [18]. Samples were incubated with primary antibody (F4/80, 1:100, or CSPG4, 1:200) at 4 °C overnight, followed by secondary antibodies (1:1000, Invitrogen) for 2 h at RT. Nuclei were counterstained with DAPI. Images were acquired using a high-resolution spinning disk confocal microscope (CREST XlightV2/VCS) involving processing 100× images with background suppression using ROI-MaxPI visualization in Nis Elements GA software.

Bone marrow-derived MP isolation

MPs isolated from bone marrow (femur and tibia) were cultivated (1×10^6) in DMEM (Catalogue No. 11965092, Gibco, Waltham, MA, USA) with 20% FBS (Catalogue No. 10270106, Gibco) 1% L-glutamine (200 mM, Catalogue No. 25030081, Gibco), 1% P/S (penicillin and streptomycin stock solution 10,000 U/ml, Catalogue No. 15140122, Gibco), 0.5% sodium pyruvate (100 mM, Catalogue No. 11360070, Gibco), 0.1% β -mercaptoethanol (Catalogue No. 21985023, Gibco), and 20 ng/ml MP-stimulating growth factor (mouse M-CSF premium grade, 130-101-700, Miltenyi Biotec, Bergisch Gladbach, Germany). After 7 days cells were stimulated with 100 ng/ml LPS (Catalogue No. L2012, Sigma-Aldrich) or 10 ng/ml IL-4 (Catalogue No. 130-097-757, Miltenyi Biotec) for 24 h to induce M1 and M2 phenotypes, respectively. MPs were analyzed by fluorescence-activated cell sorting (FACS) or co-culture experiments with chimeric antigen receptor T cells (CARTs).

3D neuro-cardiac junction generation

After 7 days differentiated WT and *mdx* MPs were treated with 40 μ g/ml of CSPG4-blocking antibody (BAb) (Santa Cruz, SC-80003) for 24 h [19]. Supernatants were collected, centrifuged at 3800 rpm (Eppendorf Centrifuge

5804R, A-4-81, Catalogue No. 5805000010), concentrated (VIVASPIN tubes cutoff 30 kDa, Catalogue No. VS0621, Sartorius, Göttingen, Germany), and equilibrated in HEPES 20 mM (1 M, Catalogue No. 15630080, Gibco) and NaCl 150 mM buffer at 3000 rpm (Eppendorf Centrifuge 5804R, A-4-81, Catalogue No. 5805000010) at 15 °C. The desalted mixture was loaded into gel filtration column chromatography for isolating chondroitin sulfate proteoglycans (CSPGs) from other protein pools. Eluted fractions with similar protein profiles were analyzed using an ELISA against CSPG4 (Catalogue No. MOEB1952, Assay Genie, Dublin, Ireland). The fractions containing CSPG4 were used for hydrogel functionalization.

Neonatal dorsal root ganglia isolation

The dorsal root ganglia (DRG) were isolated from the vertebral column of WT pups and digested in 1.25 mg/ml collagenase A (Catalogue No. 10103578001, Roche, Basel, Switzerland) and 2.5 mg/ml dispase II (Catalogue No. D4693-1G, Sigma-Aldrich) for 15 min at 37 °C. Then the pellet was resuspended in Neurobasal-A Medium (Catalogue No. 10888022, Thermo Fisher Scientific, Waltham, MA, USA), with B27 (Catalogue No. 108889038, Thermo Fisher Scientific) and 100 ng/ml nerve growth factor (NGF) 2.5S (115AFC60, Sigma-Aldrich).

Neonatal CM and cardiac fibroblast isolation

Hearts were predigested in 0.1 mg/ml trypsin (Sigma-Aldrich) overnight at 4 °C, then incubated with 0.5 mg/ml collagenase II (Catalogue No. CLS-2, Worthington Biochemical, Lakewood, NJ, USA). Cell suspensions were filtered with a 70- μ m strainer, centrifuged at 800 rpm (Eppendorf Centrifuge 5804R, A-4-81, Catalogue No. 5805000010) for 5 min at 4 °C, and resuspended in DMEM/M119 (31153-026, Gibco) medium with 5% FBS, 10% HS, 2 mM L-glutamine, and 1% P/S. Cells were plated for 3 h to allow nonmyocytes to attach, then the CM-enriched suspension was plated on 0.1% gelatin-coated dishes at 1.5×10^4 cells/cm².

3D NCJs were bio-assembled using PEG-FB as a scaffold [20,21]. Four PEG-FB bioinks were produced using MPs supernatants: WT, WT + CSPG4 BAb, *mdx*, and *mdx* + CSPG4 BAb. 18×10^6 WT CMs/ml and 6×10^6 WT CFs/ml were resuspended in bio-inks to create 100 μ l 3D bulks. Irgacure 2959 (0.01% w/v) was used as a photoinitiator (VLIG00000101, Twin Helix, London, UK), and the bulks were UV cross-linked (365 nm, 4–5 mW/cm²) for 5 min. After 24 h, 5×10^6 WT DRG were seeded on the top surface of each bulk construct and cultured in a co-culture medium with 100 ng/ml NGF for 7 days. The 3D NCJ models were fixed with 4% paraformaldehyde and stained with TUBB3 (1:100, Biolegend, San Diego, CA, USA), cTNNT (1:100, Ab8295, Abcam), and ER-TR7 (1:100, sc-73355, Santa Cruz).

Co-culture experiments with CART

Engineered CSPG4 CARTs and control (cCARTs) were provided by Dotti [22]. CARTs were maintained in Iscove's Modified Dulbecco's Medium (Catalogue No. 31980030, Gibco) with 1% P/S, 10% FBS, IL-15 (5 ng/ml, 130-095-762, Miltenyi Biotec), and IL-7 (10 ng/ml, 130-095-361, Miltenyi Biotec) for 5 days. For co-culture experiments, 1×10^4 MPs and 5×10^3 CF per cm^2 were plated in six-well plates with CSPG4. CARTs or cCART at 2:1 (effector-to-target ratio) in serum- and interleukin-free CAR-T medium. After 3 days, residual MPs and CFs were collected and evaluated by FACS for F4/80 and CD140b expression.

Flow cytometry (FACS)

MPs were incubated at 4 °C for 10 min with the following fluorochrome-conjugated antibodies: CSPG4/AN2-PE (1:100, Miltenyi Biotec, 130-116-376), F4/80-APC (1:100, Miltenyi Biotec, 130-116-547), CD11b APC/Cyanine7 (1:100, Invitrogen, 130-113-803, Carlsbad, CA, USA), CD80 eFluor450 (1:100, Invitrogen, 48-0801-82), CD206 Alexa-647 (1:100, Invitrogen, 53-2061-82), CD140b-APC-Vio770 (1:100, Miltenyi Biotec, 130-105-119). Cell viability was determined using the LIVE/DEAD fixable aqua dead cell stain kit (1:1000, Invitrogen, L34957). Data were acquired using a BD FACSCanto II flow cytometer using BD FACSDiva software (BD Biosciences, Franklin Lakes, NJ, USA) and analyzed using FlowJo version 10.8 (BD Biosciences).

FACSymphony

Hearts were predigested with 2.5 U/ml collagenase type II (Catalogue No. CLS-2, Worthington Biochemical) for 30 min at 37 °C and then centrifuged at RT for 5 min. A second incubation with 1.5 U/ml collagenase D (Catalogue No. 11088882001, Sigma-Aldrich) and dispase II (Catalogue No. 22615200, Sigma-Aldrich) was performed for 60 min. The pellet was filtered through 40- μm cell strainers and centrifuged at 1200 rpm at RT (Eppendorf Centrifuge 5804R, A-4-81, Catalogue No. 5805000010) for 5 min. Cell suspensions were incubated with Fixable stain 780 (Catalogue No. 565388, Thermo Fisher Scientific), washed, and stained with primary antibodies for 10 min on ice: CD45/BUV737 (1:100, BD Biosciences, Catalogue No. 748371, San Jose, CA, USA), CD11b /BUV563 (1:100, BD, Catalogue No. 741242), F4/80/PE-CF594 (1:100, BD Biosciences, Catalogue No. 565613), CD80/BV615 (1:100, BD Biosciences, Catalogue No. 751328), CD206/Alexa Fluor 488 (1:100, BD Biosciences, Catalogue No. 565250), Ly6C/BV605 (1:100, BD Biosciences, Catalogue No. 563011), Ly6G/BB790 (1:100, custom BD Biosciences), and CSPG4/PE (1:100, Miltenyi Biotec, Catalogue No. 130-116-440). Cells counts were acquired using a FACSymphony A5 (BD Biosciences) and analyzed by FlowJo (version 10.9). The FlowJo plugin flowAI was used for quality control and filtering out debris and nonviable cells. A random

downsampling to 5000 events per sample focused on live cells. Samples were concatenated into a dataset of 60,000 cells. Dimensionality reduction was performed using the t-SNE algorithm in FlowJo with default parameters: interaction value of 1000, perplexity value of 30, and the Barnes–Hut gradient algorithm. The gating strategy is detailed in supplementary material, Figure S1F.

Quantitative real-time PCR

Total RNA from hearts was isolated using TRIZOL reagent (Invitrogen, Life Technologies, 15596026, Carlsbad, CA, USA) following the manufacturer's instructions. Samples were treated with DNase I (Invitrogen, 2358609) following the protocol and the RNA reverse transcribed into cDNA using a TaqMan Reverse Transcription Reagents kit (Applied Biosystems, N8080234, Foster City, CA, USA). Gene expression was evaluated by quantitative real-time PCR (RT-qPCR) with SYBR green (SensiFAST SYBR Lo-ROX kit, Meridian Bioscience, BIO-94005, Cincinnati, OH, USA) on a Real-Time PCR Instrument (A28135 A28140, Applied Biosystems Quantstudio 5 real-time PCR system). The thermal cycling conditions for all primers (supplementary material, Table S2) were as follows: 2 min at 50 °C, 10 min at 95 °C, and 40 cycles of 15 s at 95 °C and 1 min at 60 °C. Data are presented as relative expression normalized to the reference transcript *EIF2A* and the WT group as control.

Western blot

Proteins were extracted from tissues using lysis buffer (50 mM TRIS HCl pH 7.5), 0.6 M sucrose (Catalogue No. S0389, Sigma-Aldrich), 50% glycerol (Catalogue No. G5516, Sigma-Aldrich), 1% TRITON, 50 mM NaCl, 10 mM NaF, 2 mM sodium orthovanadate (Na_3VO_4 , Catalogue No. 450243 Sigma-Aldrich), 1 mM PMSF (Catalogue No. 36978, Thermo Scientific, Waltham, MA, USA), 5 mM β -glycerophosphate (Catalogue No. G9422, Sigma-Aldrich), 1000X protease inhibitors (Catalogue No. 04693116001, Roche) for 30 min on ice, sonicated, and centrifuged at $12,000 \times g$ for 15 min at 4 °C. Proteins were resolved using SDS-PAGE, transferred to nitrocellulose membranes (Catalogue No. GE10600079, Amersham Protran, Johns Creek, GA, USA), blocked with 5% nonfat dry milk powder (Catalogue No. 1.15363, Merck Millipore, Billerica, MA, USA) in PBS $1 \times$ for 45 min, and incubated at 4 °C overnight with primary antibodies: tyrosine hydroxylase (1:1000, ab152), Synapsin 1 (1:1000, Cell Signaling Technology, #5297), CSPG4 (1:1000, Cell Signaling Technology, #52635), and Vinculin (1:500, V9131, Sigma-Aldrich), followed by incubation with secondary antibodies (anti-Rabbit NA934AV, 1:5000; anti-Mouse LNXa931/AE, 1:10000, GE Healthcare Life Sciences, Havelock, NE, USA) for 1 h at RT. Immunocomplexes were detected by chemiluminescence (ECL kit; Merck Millipore) and analyzed by densitometry using ImageJ.

Statistics

GraphPad Prism Software (version 8.4.2; GraphPad, Boston, MA, USA) was used for graphing and statistical analysis. Data were expressed as mean \pm SEM. Significance for two experimental groups was determined using unpaired single-tail Student's *t*-tests, whereas differences among more groups were calculated as one-way and two-way ANOVA with multiple comparisons testing (Tukey). *p* values: **p* < 0.05, ***p* < 0.01, ****p* < 0.001, *****p* < 0.0001.

Results

Increased fibrosis and NCJ alterations in dystrophic hearts

Histological analysis of cardiac tissues from young and aged (3 and 10 months, respectively) *mdx* mice (a DMD model) confirmed severe and progressive ventricular fibrosis, with a higher fibrotic index compared to WT (Figure 1A). Genes encoding for collagen 1 and 3 (*Col1a1*, *Col3a1*) and fibronectin (*Fn1*), associated with fibrosis cardiac tissue stiffness [23], were significantly upregulated in both young and aged dystrophic mice with respect to controls (Figure 1B). However, *Tgfb1* and transcription factors *Twist1* and *Twist2*, involved in collagen production and ECM deposition [24], were significantly increased only in aged dystrophic mice (Figure 1B).

Confocal microscopy revealed a disorganized distribution of synaptic terminals and a decreased percentage of the positive area to TH and SYN1 (markers of dopaminergic neurons and synaptic vesicles, respectively) in *mdx* mice at 3 and 10 months (Figure 1C,D). Interestingly, the percentage of the positive area for F4/80 (a unique marker of mouse microglia and MPs) significantly and progressively increased in both young and mainly in adult *mdx* mice (Figure 1C,D). Notably, CSPG4 staining was observed both around and overlapped on F4/80 positive cells within the fibrotic area labeled with Fn1 antibody (Figure 1C). Western blotting analysis confirmed increased CSPG4 and decreased TH and SYN1 in both young and aged *mdx* mice (Figure 1E,F).

Bone marrow-derived MPs can produce CSPG4

Given the concurrent presence of MPs and CSPG4 in the cardiac tissue of *mdx* mice, we investigated whether MPs produced CSPG4. Bone marrow-derived monocytes (essential for muscle regeneration in DMD and known contributors of CSPG4 [25]) from both WT and *mdx* mice were differentiated *in vitro* into three MP phenotypes (M0, M1, M2) by means of LPS and IL-4 (supplementary material, Figure S1A,B). CSPG4 expression in these phenotypes was confirmed by FACS analysis and high-resolution immunofluorescence (supplementary material, Figure S1C–E). Next, we co-cultured the M0, M1, and M2 populations with the engineered CARTs targeting CSPG4 (CSPG4-CARTs), designed to exert

cytolytic activity against cells expressing CSPG4. The CSPG4-CARTs showed significantly increased cytolytic activity toward all MP populations (Figure 2A). Cardiac fibroblasts (CFs), known producers of proteoglycans in the cardiac tissue [26], did not reproduce this effect (Figure 2A). Supernatants from WT and aged dystrophic MP-derived cultures were tested for CSPG4 levels by ELISA, which revealed that old *mdx* mice MPs excreted higher CSPG4 levels than WT (Figure 2B).

Additionally, cardiac tissues from young and old WT and *mdx* mice were analyzed using FACSymphony. The unsupervised analysis was performed on the same number of events per sample (15,000 events for experimental groups) (tSNE scatter plot, Figure 2C, top), representing the distribution of concatenated total cells of all experimental groups (blue and greenish for 3- and 10-month-old *mdx*; orange and magenta for 3- and 10-month-old WT), and showed that the cluster of myeloid cells (dark pink, Figure 2C, bottom) was more enriched between young and old *mdx* mice compared to WT.

The deep analysis revealed a higher percentage of total MPs positive for CSPG4 (F4/80^{pos}/CSPG4^{pos}) in *mdx* mice at both 3 and 10 months of age compared to controls (Figure 2D). A focused analysis of MP subpopulations showed a significant increase in M2 (CD206^{pos}/CSPG4^{pos}), resident MPs (Ly6C^{low}/CSPG4^{pos}), and recruited monocytes (Ly6C^{high}/CSPG4^{pos}) [27] in young dystrophic mice compared to controls (Figure 2E). A nonsignificant trend was observed in the pro-inflammatory M1 subset (Figure 2E). In aged mice, higher percentages of M1 (CD80^{high}/CSPG4^{pos}) and recruited monocytes (Ly6C^{high}/CSPG4^{pos}) were found (Figure 2E).

CSPG4 released by MP-inhibited axon growth in a 3D model of NCJ

To verify the effect of CSPG4 released by MPs on the biological cross-talk between the heart and nervous system, we recapitulated *in vitro* NCJ using 3D multicellular constructs.

Supernatants of WT and *mdx* MPs, untreated or treated with CSPG4-blocking antibody (BAB), were employed to reconstitute polyethylene glycol-fibrinogen (PEG-FB) biomaterial. Four 3D NCJ models were generated: WT, WT + CSPG4 BAB, *mdx*, and *mdx* + CSPG4 BAB. The NCJ consisted of neonatal CMs and CFs isolated from pups, embedded in conditioned PEG-FB. DRG were plated on the top of the 3D structures (Figure 3A). We quantified the area occupied by TUBB3-labeled neuron endings (24) within the 3D models. Results showed a significant restoration in the *mdx* 3D NCJ treated with CSPG4 BAB compared to untreated *mdx* 3D NCJ (Figure 3C,D). The growth of DRG in the *mdx* 3D NCJ was inhibited with respect to WT, as expected (Figure 3C,D). The result confirmed that CSPG4 released from dystrophic MPs altered the communication between cardiac tissue and synaptic terminals by paracrine activity.

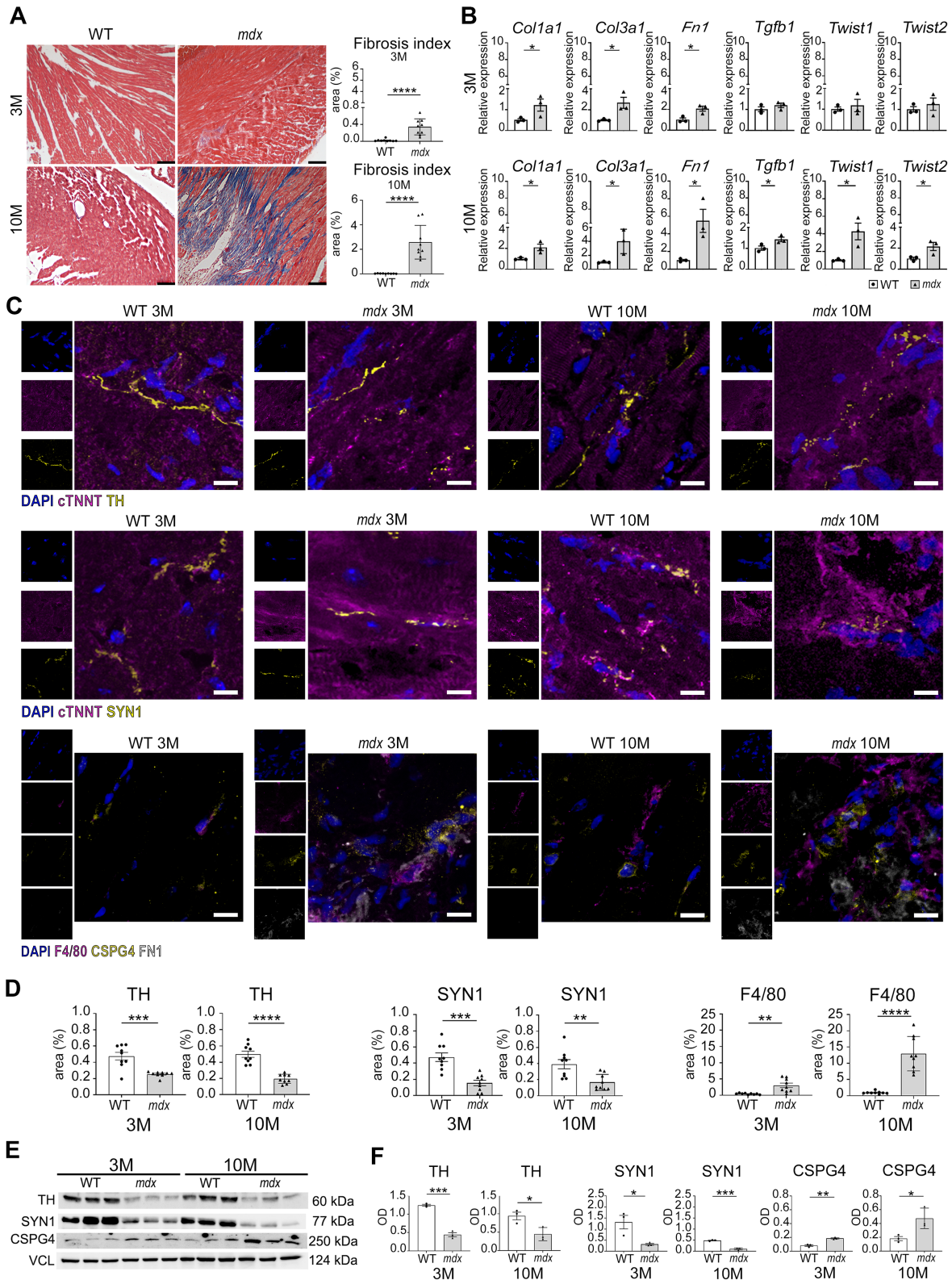


Figure 1. Cardiac fibrosis and innervation. (A) Masson's trichrome staining of young (3-month-old) and old (10-month-old) WT and *mdx* mouse hearts. Scale bars, 100 μ m. The graph shows the area as a percentage of the fibrosis index (fibrotic area/whole area). $N = 3$ biological replicates. (B) qPCR for fibrosis-related transcripts in 3- and 10-month-old *mdx* and WT hearts (*Col1a1*, *Col3a1*, *Fn1*, *Tgfb1*, *Twist1*, *Twist2*). $N = 3$ biological replicates. (C) Confocal images for tyrosine hydroxylase (TH), Synapsin 1 (SYN1), MPs (F4/80), proteoglycan CSPG4, and fibronectin 1 (FN1) on myocardium sections of 3- and 10-month-old mice. The markers TH, SYN1, and CSPG4 are labeled in yellow, cardiac troponin (cTNNT) and F4/80 are in magenta, while FN1 is in white. Scale bars, 10 μ m. Nuclei are counterstained with DAPI in blue. (D) Charts indicate positive area expressed as percentage of TH, SYN1, and F4/80 on whole area. $N = 3$ sections per $N = 3$ biological replicates. (E and F) Western blot analysis of TH, SYN1, and CSPG4 in *mdx* and WT hearts of young and old mice. Graphs show optical density (OD) of protein bands normalized to vinculin (VCL). $N = 3$ biological replicates. Error bars show SEM. * $p < 0.05$, ** $p < 0.01$, *** $p < 0.001$, **** $p < 0.0001$ were calculated using Student's *t*-test.

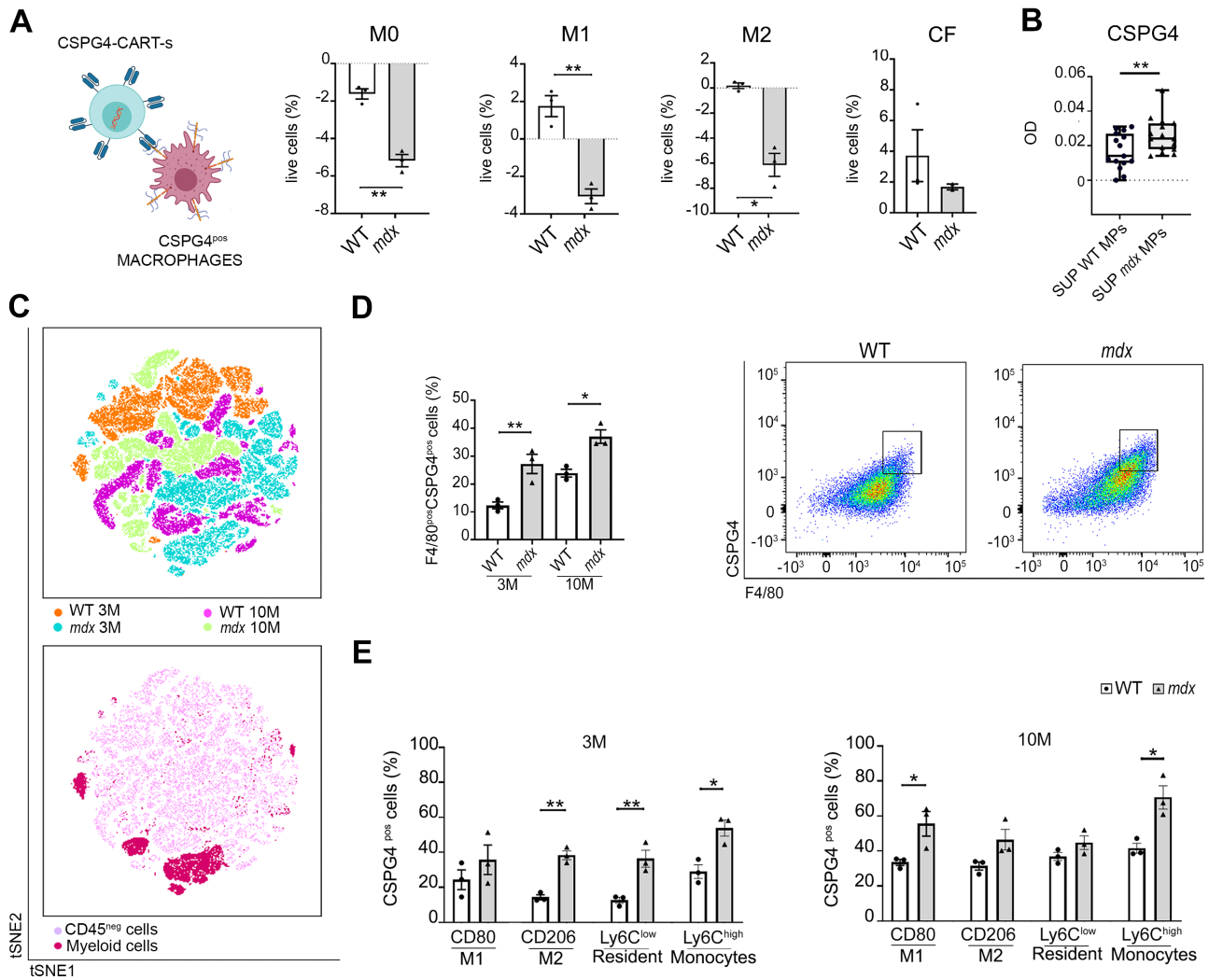


Figure 2. MPs as main producers of CSPG4. (A) Graphic illustration of CSPG4-CAR-Ts cells against MPs expressing CSPG4. Created with [Biorender.com](https://www.biorender.com). Diagrams quantifying the percentage of live cells of bone marrow-derived MPs of both WT and *mdx* M0 (nonactivated), M1 (pro-inflammatory) and M2 (anti-inflammatory), or CFs after exposure to CSPG4.CARTs compared to cells co-cultured with control CART (cCART). *N* = 3 biological replicates. (B) ELISA assay for CSPG4 in supernatants (SUP) isolated from WT and *mdx* MPs. The chart illustrates the optical density (OD) of CSPG4 in the two groups. Each dot represents the eluted fractions, *N* = 16. (C) FACSymphony of cardiac tissues. The first chart represents a scatter plot of t-SNE relative to concatenated total cells from 3- or 10-month-old WT and *mdx* hearts. The second chart illustrates the distribution of CD45^{neg} cells (light pink cluster) and myeloid cells (dark pink cluster) in all groups. (D) Graph of FACS analysis relative to number of total MPs (F4/80) positive for CSPG4 in 3- or 10-month-old WT and *mdx* hearts. (E) Expression of CSPG4 in subpopulations of MPs: CD80^{pos} (M1), CD206^{pos} (M2), Ly6C^{low} (resident), and Ly6C^{high} (monocytes) in 3- or 10-month-old WT and *mdx* hearts. Error bars show SEM. **p* < 0.05, ***p* < 0.01 calculated using Student's *t*-test and one-way ANOVA.

Givinostat modulates CSPG4 and MP phenotype and enhances cardiac function

As we previously demonstrated, givinostat, a pan-histone deacetylase inhibitor currently in phase III clinical trial for DMD [28], effectively reduces inflammation and cardiac fibrosis [16]. We investigated whether givinostat also affected CSPG4 in the heart and modulated the MP phenotype. Results showed that givinostat significantly enhanced the percentage of the positive area to both TH and SYN1 in the cardiac tissue of aged *mdx* mice compared to the untreated dystrophic group (Figure 4A,B). Additionally, there was a significant decrease in the MP-covered area (F4/80^{pos}) around and overlapping CSPG4 in the fibrotic regions of aged *mdx* treated with givinostat with

respect to the *mdx* saline group (Figure 4A,B). Staining for TH revealed intact synaptic terminals in WT, unlike disorganized distribution within the fibrotic area in *mdx* mice overlapping with MPs and CSPG4 (Figure 4A, lower panel). Similar results were observed in young *mdx* mice with a decrease in F4/80 positive area (supplementary material, Figure S2A,B). FACSymphony showed a significant reduction of the percentage of CSPG4^{pos} MPs positive in cardiac tissues of young and aged *mdx* mice treated with givinostat compared to controls (supplementary material, Figure S2C).

Western blot analysis confirmed these results (Figure 4C,D). Importantly, *Th*, high- and low-affinity *Ngf* receptors, neurotrophic receptor tyrosine kinase

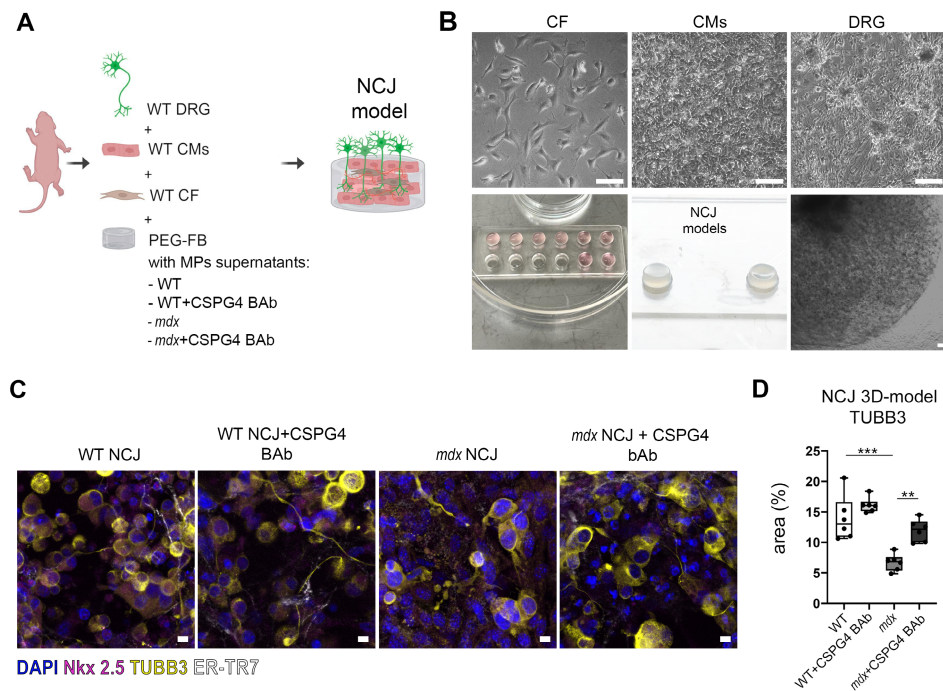


Figure 3. MPs release CSPG4 in media and inhibit axon growth of dorsal root ganglia. (A) Rendering of 3D NCJ generation. The picture was created with [Biorender.com](#) and illustrates the composition of the 3D NCJ model: WT dorsal root ganglia (DRG), WT cardiomyocytes (CMs), and WT CFs were encapsulated in PEG-FB hydrogel conditioned with the supernatants derived from MP cultures of WT, WT + CSPG4 blocking antibody (BAb), *mdx*, and *mdx* + CSPG4 (BAb). (B) Brightfield images of CFs, CMs, and DRG after 1 day of culture (upper panel) and 3D constructs of NCJ models after 7 days (lower panel). Scale bars, 100 μ m. (C) Confocal images of 3D NCJ models: WT, WT + CSPG4 BAb, *mdx*, *mdx* + CSPG4 BAb. DRG are labeled with tubulin beta 3 (TUBB3, in yellow), CMs with cardiac troponin (cTNNT, in magenta), and CFs with fibroblast marker (ER-TR7, in white). (D) The graph indicates the area (%) occupied by neuron endings labeled by TUBB3 inside the 3D NCJ models. $N = 3$ biological replicates, $N = 2$ sections/constructs. Scale bars, 10 μ m. ** $p < 0.01$, *** $p < 0.001$ were determined using one-way ANOVA.

1 (*Ntrk1*), and nerve growth factor receptor (*Ngfr*) were upregulated in DRG isolated from aged dystrophic mice treated with givinostat (Figure 4E), while *Tubb3* levels remained unaltered (Figure 4E).

Connexin-43 expression, crucial for myocardial gap junction formation and overexpressed in dystrophic pathology [29], was restored in aged *mdx* animals after givinostat treatment (Figure 5A,B).

Cardiac fibrotic area and phenotype significantly reduced (Figure 5C,D), with downregulated transcriptional levels of *Tgfb1*, *Col1a1*, *Col3a1*, *Twist1*, *Twist2*, *Fnl1*, *Cspg4*, *Chst11* (the enzyme catalyzing the transfer of sulfate groups on CSPG4 chains), *Adgre1*, and *Mmp9* (Figure 5E). Givinostat had no such effect in young mice (supplementary material, Figure S3A,B).

Echocardiographic analysis showed functional heart recovery with significant enhancement of the fractional shortening (FS) and ejection fraction (EF) in aged *mdx* mice upon givinostat treatment (Figure 6A,B). Furthermore, left ventricular end-diastolic (LVEDV) and stroke volume (LVESV) indicated cardiac remodeling changes (supplementary material, Table S1). Hemodynamic analysis confirmed improved systolic function in the *mdx* givinostat group, with recovery of end-systolic pressure (P_{es}), maximum pressure (P_{max}), and maximum and minimum rate of pressure change (Max Dp/Dt and Min Dp/Dt) (Figure 6C). No significant changes in body weight, heart weight, or ratio of heart weight to tibia length were found

between givinostat-treated and *mdx* saline groups (supplementary material, Figure S4A).

Discussion

CSPG4 is expressed at peripheral nerves and triggers cytoskeletal rearrangements [30]. The role of CSPG4 in the cardiac tissue of DMD has not been previously explored. Only a few studies have reported the upregulated expression of CSPG4 in the sarcolemma and the neuromuscular junction of human postnatal skeletal muscle in DMD and other severe dystrophies [31–33].

CSPG4 is also a marker for mesenchymal progenitor cells involved in fibroblast/adipogenic differentiation in skeletal muscle [34]. The accumulation of CSPG4 is recognized to inhibit the progression of nerve endings within the heart. However, our study is the first to show CSPG4 overproduction at NCJ in *mdx* mice cardiac tissue, with CSPG4 protein levels increasing with age. Older *mdx* mice show higher CSPG4 production than their young counterparts, whereas in human dystrophic skeletal muscles, CSPG4 expression inversely correlates with age [33], suggesting differences between skeletal and cardiac tissue and between murine and human models.

Our data confirm that MP-driven inflammatory processes are dysregulated in DMD: both pro- and anti-inflammatory MP responses are imbalanced,

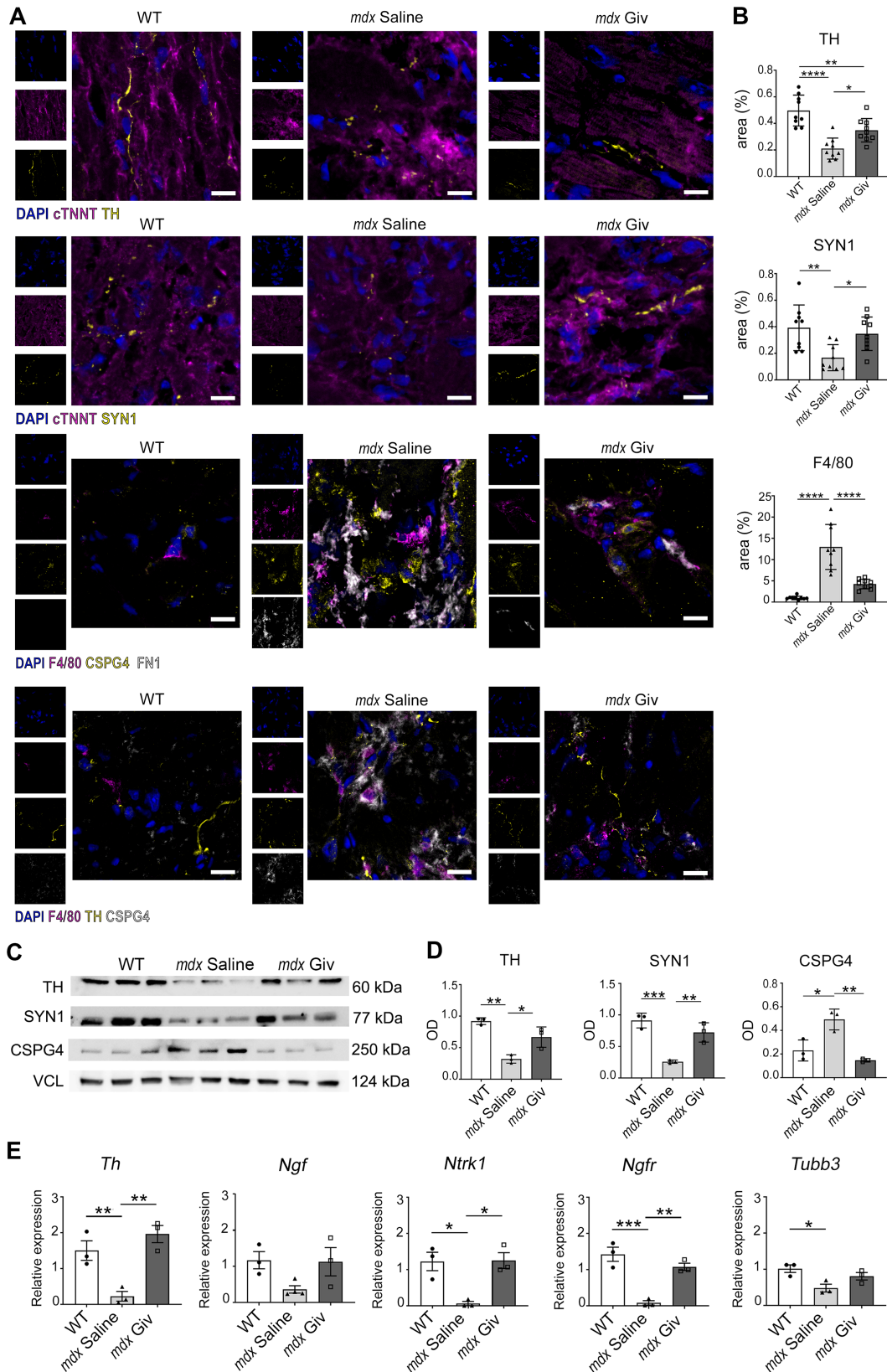


Figure 4. Cardiac innervation in old *mdx* and WT mice. (A) Immunofluorescence staining for tyrosine hydroxylase (TH), Synapsin 1 (SYN1), total MPs (F4/80) and proteoglycan (CSPG4), fibronectin 1 (FN1) on cardiac sections from 10-month-old mice. The markers TH and SYN1 are labeled in yellow, while cardiac troponin (cTNNT) and F4/80 are in magenta, FN1 in white, and CSPG4 in yellow or white. DAPI nuclear counterstaining is in blue. Scale bars, 10 μ m. (B) Charts indicate area expressed as percentage of TH, SYN1, and F4/80 (positive area/whole area). $N = 3$ sections per $N = 3$ biological replicates. (C and D) Western blot analysis for TH, SYN1, and CSPG4 quantified as optical density (OD) of protein bands normalized to vinculin (VCL). $N = 3$ biological replicates. (E) qPCR relative to markers for neurotransmitter production (*Th*), survival (*Ngf*, *Ntrk1*, and *Ngfr*) and axon guidance (*Tubb3*) in DRG. $N = 3$ biological replicates. Error bars show SEM. * $p < 0.05$, ** $p < 0.01$, *** $p < 0.001$, **** $p < 0.0001$ were calculated using one-way ANOVA.

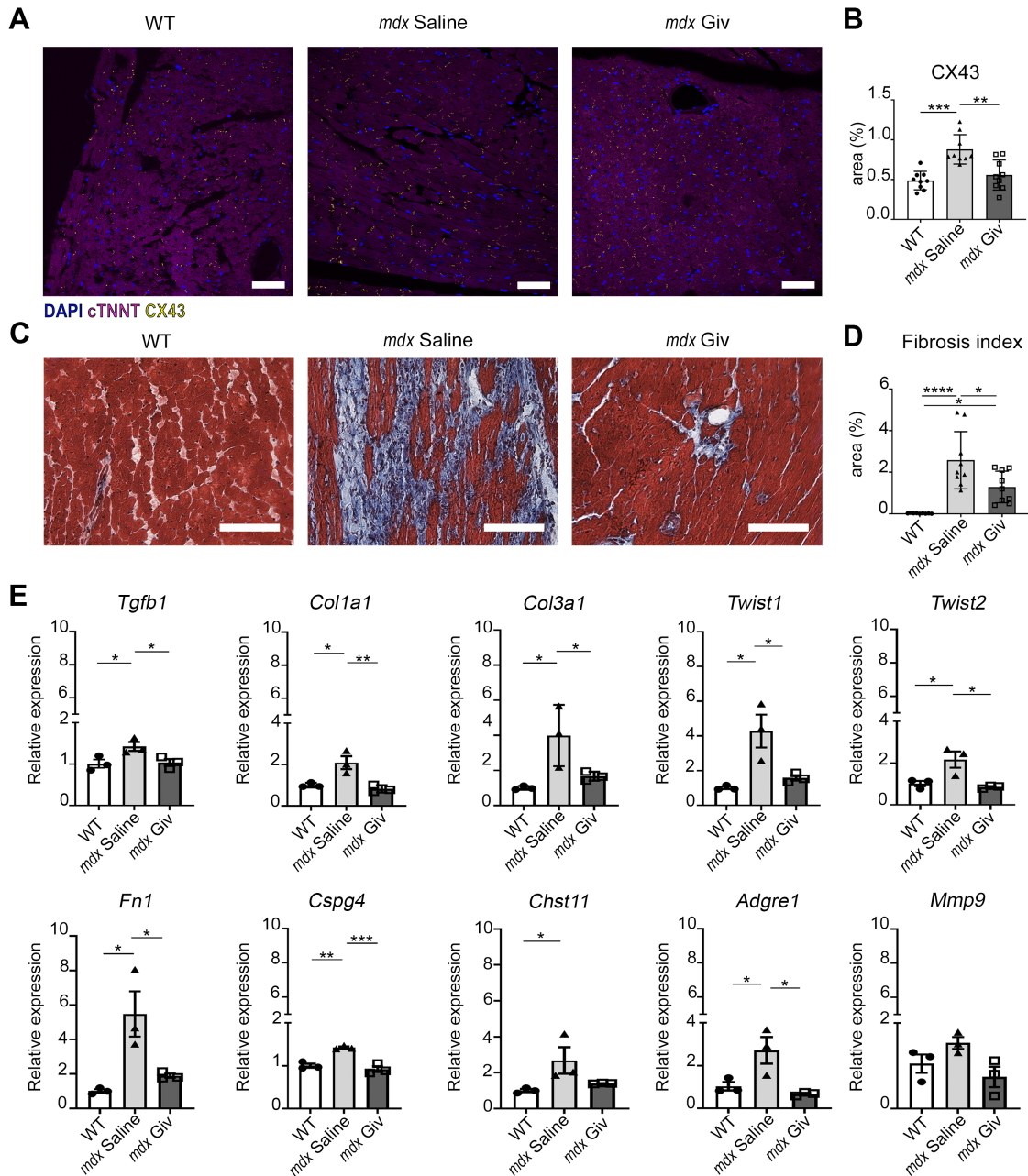


Figure 5. Histological analysis and gene profile of cardiac tissue after treatment with givostat in old *mdx* and WT mice. (A) Confocal images of immunostaining for gap junctions (CX43) and cardiomyocytes positive for cardiac troponin (cTnNT), $N = 3$ sections per $N = 3$ biological replicates. Scale bars, 50 μm . (B) Charts indicate area as percentage of CX43 (positive area/whole area). (C and D) Representative Masson's trichrome images of WT, *mdx* saline, and *mdx* Giv hearts and fibrosis index quantification (fibrotic area/whole area) after 60 days of treatment. Scale bars, 100 μm . $N = 3$ biological replicates. (E) qPCR of fibrosis-related genes (*Tgfb1*, *Col1a1*, *Col3a1*, *Twist1*, *Twist2*, *Fn1*), cell surface proteoglycan (*Cspg4*); the enzyme catalyzes the transfer of sulfate groups on CSPG4 chains (*Chst11*) and inflammatory markers (*Adgre1* and *Mmp9*). $N = 3$ biological replicates. Error bars show SEM. * $p < 0.05$, ** $p < 0.01$, *** $p < 0.001$, **** $p < 0.0001$ were calculated using one-way ANOVA and Student's *t*-test.

dynamic, and disease-stage-specific [35]. MPs are the most important cell population found altered in human dystrophic skeletal muscles of human patients and *mdx* mice. The role of MP subsets is still debated and tissue-dependent due to different signals within the inflammatory microenvironment, polarizing the inflammatory response. Our study focused on cardiac MPs modulating CSPG4 and their contribution to fibrosis. While CSPG4 is expressed in all MP populations, our data highlight that the percentages of different subsets positive for

CSPG4 in dystrophic mice hearts vary with disease progression. In young dystrophic mice, all subsets contribute to CSPG4 expression, coherent with the necrotic phase of the disease [36] as the cardiac tissue attempts to accelerate repair. In aged mice (late stage of the disease for the *mdx* model) [37], we observed a chronic inflammatory phase characterized by a higher percentage of the pro-inflammatory M1 MPs and a higher percentage of Ly6C^{high} marker, indicating persistent recruitment of bone marrow-derived monocytes. This suggests a

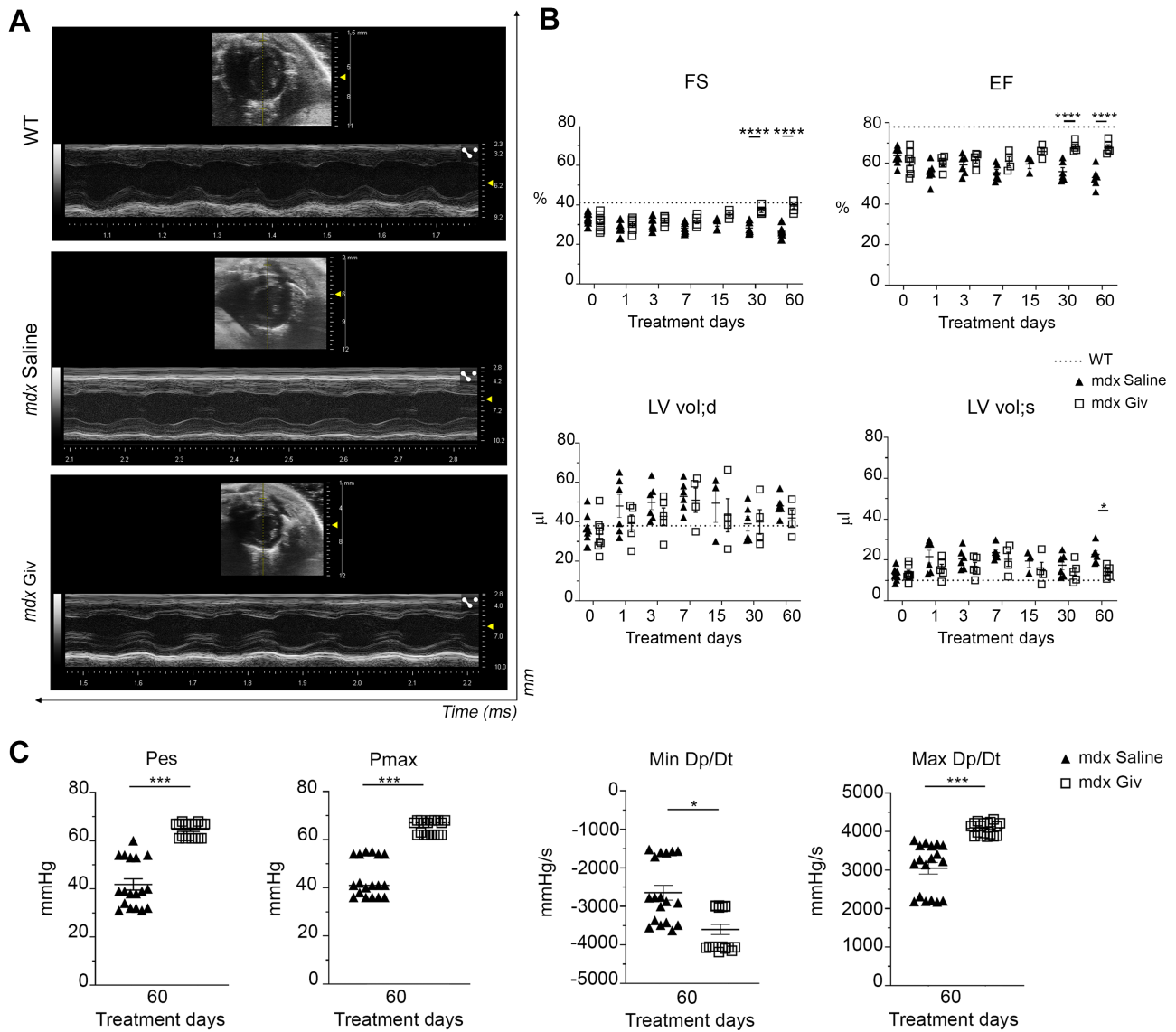


Figure 6. Impact of givinostat on dystrophic cardiomyopathy. (A) Echocardiographic M-mode images of parasternal long axis view of anterior and posterior walls of left ventricle of WT, *mdx* saline, and *mdx* Giv (Vevo 3100, VisualSonics). (B) Echocardiographic parameters: fractional shortening (FS), ejection fraction (EF), and left ventricular end-diastolic/systolic volume (LV vol;d LV vol;s) in 10-month-old mice. The x-axis shows givinostat or saline treatment on different days (0, 1, 3, 7, 30, and 60). A range of a minimum of three to a maximum of six biological replicates. (C) Hemodynamic analysis including end-systolic pressure (P_{es}), maximum pressure (P_{max}), minimum rate of pressure change (Min Dp/Dt), and maximum (Max Dp/Dt). $N = 3$ biological replicates, $N = 6$ measurements/mouse. Error bars show SEM. * $p < 0.05$, ** $p < 0.01$, *** $p < 0.001$, **** $p < 0.0001$ were calculated using two-way ANOVA.

chronic progression of the inflammatory process, driven by MPs in early disease stages, fostering progressive accumulation of CSPG4, unfavorable ECM remodeling, and disrupted NCJ communication. As DMD progresses, the pro-inflammatory and recruiting MP phenotype dominates, negatively impacting cardiac function and generating dilated cardiomyopathy, a delayed phenomenon in *mdx* mice [38,39]. Notably, our data indicate that the dystrophic MPs' ability to excrete CSPG4 has a paracrine effect on the cardiac microenvironment, reducing synaptic terminals in the 3D model of NCJ. However, it remains unclear whether denervation precedes dilated cardiomyopathy and fibrosis or whether these events occur concurrently. Denervation likely follows

inflammatory damage, with CSPG4 as the biological mediator. Accordingly, after ischemia-reperfusion injury, the infarcted area shows sympathetic denervation, increased CSPG4, and inhibited axon growth [40]. In other contexts, pathological tissue inflammation upregulates MPs expressing CSPG4 [41].

Previously, we demonstrated that givinostat reduced inflammation and fibrosis in a mouse model of acute myocardial infarction, improving cardiac performance [16]. The impact of givinostat on dystrophic dilated cardiomyopathy is still unknown. We have already shown that givinostat has a broad-spectrum and anti-inflammatory effect with anti-fibrotic consequences [16]. The present study demonstrates that by decreasing MP-

driven inflammation, givinostat also reduces the content of CSPG4 in dystrophic cardiac tissue. The effect of givinostat on the NCJ is likely indirect, fostering a favorable microenvironment for restoring cardiac sympathetic innervation, crucial for cardiac repair, regeneration, and function [42].

We observed cardiac function improvement within 30–60 days, consistent with the *mdx* preclinical model pathophysiology [43]. We speculate that givinostat might exert a long-term stabilizing action on cardiac function, parallel to a sustained reduction of cardiac inflammation and fibrosis over time.

Conclusions

We cannot exclude that additional partners such as microvasculature-associated vascular mural cells [44,45] and adult cardiac pericytes [46] may contribute to CSPG4 release, beyond MPs in dystrophic cardiac tissue, contributing to ECM deposition.

Our data offer insights into the interplay among inflammation, fibrosis, and the nervous system in cardiomyopathy, identifying new pharmacological targets.

Acknowledgements

This work was supported by Fondazione Regionale per la Ricerca Biomedica (Regione Lombardia), Project ID 1731651; Italian Ministry of Health, Project starting grant code SG-2019-12368961; Duchenne Parent Project ONLUS (Italy); ITALFARMACO; Fondazione ROCHE (nonconditional contribution). The authors thank Fondazione Roma for the VisualSonics Vevo 3100. EDF is supported by the grant Progetto ECS 0000024 Rome Technopole, CUP B83C2200282000820006, PNRR Missione 4 Componente 2 Investimento 1.5, funded by the European Union—Next Generation EU.

Author contributions statement

RR conceptualized the study and designed the experiments. RR and CB acquired funding for the project and supervised all generation, collection, and analyses of research data. MM performed all the experiments, analyzed the data and prepared the figures and tables. RR, CB, EDF and MM wrote and edited the manuscript. FM, MC, RZ, VDP, NF, CP, MT and MB conducted the *in vitro* experiments and supported in data analysis. AS, SM, FM and MC performed the *in vivo* experiments. EL and GD provided CAR-T cells. MGC and MC conducted experiments using flow cytometry and analyzed the data. CC carried out high-resolution immunofluorescence on cells. DS supplied biomaterial for the 3D culture. DDS, FB, PM, AC, YT, CL and EDF provided experimental support. All authors approved the final version of the manuscript.

Data availability statement

The data that support the findings of this study are available from the corresponding author upon reasonable request.

References

- Nowak KJ, Davies KE. Duchenne muscular dystrophy and dystrophin: pathogenesis and opportunities for treatment. *EMBO Rep* 2004; **5**: 872–876.
- Lombardi L, Stefano MED, Paggi P. Components of the NGF signaling complex are altered in *mdx* mouse superior cervical ganglion and its target organs. *Neurobiol Dis* 2008; **32**: 402–411.
- Shannon TR. Ryanodine receptor Ca^{2+} sensitivity and excitation-contraction coupling in muscular dystrophy and heart failure: similar and yet different. *Am J Physiol Heart Circ Physiol* 2009; **297**: H1965–H1966.
- Canonica F, Chirivi M, Maiullari F, et al. Focus on the road to modelling cardiomyopathy in muscular dystrophy. *Cardiovasc Res* 2022; **118**: 1872–1884.
- Tripodi L, Villa C, Molinaro D, et al. The immune system in Duchenne muscular dystrophy pathogenesis. *Biomedicines* 2021; **9**: 1447.
- Kharraz Y, Guerra J, Pessina P, et al. Understanding the process of fibrosis in Duchenne muscular dystrophy. *Biomed Res Int* 2014; **2014**: 1–11.
- Tulangekar A, Sztal TE. Inflammation in Duchenne muscular dystrophy—exploring the role of neutrophils in muscle damage and regeneration. *Biomedicines* 2021; **9**: 1366.
- Gallardo FS, Córdova-Casanova A, Brandan E. The linkage between inflammation and fibrosis in muscular dystrophies: the axis autotaxin-lysophosphatidic acid as a new therapeutic target? *J Cell Commun Signal* 2021; **15**: 317–334.
- Klingler W, Jurkat-Rott K, Lehmann-Horn F, et al. The role of fibrosis in Duchenne muscular dystrophy. *Acta Myol* 2012; **31**: 184–195.
- Bez Batti Angulski A, Hosny N, Cohen H, et al. Duchenne muscular dystrophy: disease mechanism and therapeutic strategies. *Front Physiol* 2023; **14**: 1183101.
- Rüdolf R, Khan MM, Labeit S, et al. Degeneration of neuromuscular junction in age and dystrophy. *Front Aging Neurosci* 2014; **6**: 99.
- Brescia M, Chao Y-C, Koschinski A, et al. Multi-compartment, early disruption of cGMP and cAMP signalling in cardiac myocytes from the *mdx* model of Duchenne muscular dystrophy. *Int J Mol Sci* 2020; **21**: 7056.
- Ilieva KM, Cheung A, Mele S, et al. Chondroitin sulfate proteoglycan 4 and its potential As an antibody immunotherapy target across different tumor types. *Front Immunol* 2017; **8**: 1911.
- Sakry D, Neitz A, Singh J, et al. Oligodendrocyte precursor cells modulate the neuronal network by activity-dependent ectodomain cleavage of glial NG2. *PLoS Biol* 2014; **12**: e1001993.
- Ng SY, Ljubcic V. Recent insights into neuromuscular junction biology in Duchenne muscular dystrophy: impacts, challenges, and opportunities. *EBioMedicine* 2020; **61**: 103032.
- Milan M, Pace V, Maiullari F, et al. Givinostat reduces adverse cardiac remodeling through regulating fibroblasts activation. *Cell Death Dis* 2018; **9**: 108.
- Pegoli G, Milan M, Manti PG, et al. Role of *Cdkn2a* in the Emery-Dreifuss muscular dystrophy cardiac phenotype. *Biomolecules* 2021; **11**: 538.
- De Paolis V, Maiullari F, Chirivi M, et al. Unusual association of NF- κ B components in tumor-associated macrophages (TAMs) promotes HSPG2-mediated immune-escaping mechanism in breast cancer. *Int J Mol Sci* 2022; **23**: 7902.

19. Sardone F, Santi S, Tagliavini F, *et al.* Collagen VI-NG2 axis in human tendon fibroblasts under conditions mimicking injury response. *Matrix Biol* 2016; **55**: 90–105.
20. Chirivì M, Maiullari F, Milan M, *et al.* Tumor extracellular matrix stiffness promptly modulates the phenotype and gene expression of infiltrating T lymphocytes. *Int J Mol Sci* 2021; **22**: 5862.
21. Maiullari F, Costantini M, Milan M, *et al.* A multi-cellular 3D bioprinting approach for vascularized heart tissue engineering based on HUVECs and iPSC-derived cardiomyocytes. *Sci Rep* 2018; **8**: 13532.
22. Pellegatta S, Savoldo B, Ianni ND, *et al.* Constitutive and TNF α -inducible expression of chondroitin sulfate proteoglycan 4 in glioblastoma and neurospheres: implications for CAR-T cell therapy. *Sci Transl Med* 2018; **10**: ea02731.
23. Cowling RT, Kupsky D, Kahn AM, *et al.* Mechanisms of cardiac collagen deposition in experimental models and human disease. *Transl Res* 2019; **209**: 138–155.
24. Xu J, Lamouille S, Derynck R. TGF-beta-induced epithelial to mesenchymal transition. *Cell Res* 2009; **19**: 156–172.
25. Liu Y, Hammel G, Shi M, *et al.* Myelin debris stimulates NG2/CSPG4 expression in bone marrow-derived macrophages in the injured spinal cord. *Front Cell Neurosci* 2021; **15**: 651827.
26. Hall C, Gehmlich K, Denning C, *et al.* Complex relationship between cardiac fibroblasts and cardiomyocytes in health and disease. *J Am Heart Assoc* 2021; **10**: e019338.
27. Yang P, Liu L, Sun L, *et al.* Immunological feature and transcriptional signaling of Ly6C monocyte subsets from transcriptome analysis in control and Hyperhomocysteinemic mice. *Front Immunol* 2021; **12**: 632333.
28. Mercuri E, Vilchez JJ, Boespflug-Tanguy O, *et al.* Safety and efficacy of givinostat in boys with Duchenne muscular dystrophy (EPIDYS): a multicentre, randomised, double-blind, placebo-controlled, phase 3 trial. *Lancet Neurol* 2024; **23**: 393–403.
29. Gonzalez JP, Ramachandran J, Himelman E, *et al.* Normalization of connexin 43 protein levels prevents cellular and functional signs of dystrophic cardiomyopathy in mice. *Neuromuscul Disord* 2018; **28**: 361–372.
30. Nicolosi PA, Dallatomasina A, Perris R. Theranostic impact of NG2/CSPG4 proteoglycan in cancer. *Theranostics* 2015; **5**: 530–544.
31. Maciej-Hulme ML, Melrose J, Farrugia BL. Arthritis and Duchenne muscular dystrophy: the role of chondroitin sulfate and its associated proteoglycans in disease pathology and as a diagnostic marker. *Am J Physiol Cell Physiol* 2023; **324**: C142–C152.
32. Blake MR, Parrish DC, Staffenson MA, *et al.* Chondroitin sulfate proteoglycan 4,6 sulfation regulates sympathetic nerve regeneration after myocardial infarction. *Elife* 2022; **11**: e78387.
33. Petrini S, Tessa A, Carrozzo R, *et al.* Human melanoma/NG2 chondroitin sulfate proteoglycan is expressed in the sarcolemma of postnatal human skeletal myofibers. Abnormal expression in merosin-negative and Duchenne muscular dystrophies. *Mol Cell Neurosci* 2003; **23**: 219–231.
34. Takeuchi S, Nakano S-I, Nakamura K, *et al.* Roles of chondroitin sulfate proteoglycan 4 in fibrogenic/adipogenic differentiation in skeletal muscle tissues. *Exp Cell Res* 2016; **347**: 367–377.
35. Petrof BJ. Macrophage plasticity in Duchenne muscular dystrophy: a nexus of pathological remodelling with therapeutic implications. *J Physiol* 2022; **600**: 3455–3464.
36. Morotti M, Garofalo S, Coccozza G, *et al.* Muscle damage in dystrophic mdx mice is influenced by the activity of Ca²⁺-activated K_{Ca}3.1 channels. *Life (Basel)* 2022; **12**: 538.
37. Li W, Liu W, Zhong J, *et al.* Early manifestation of alteration in cardiac function in dystrophin deficient mdx mouse using 3D CMR tagging. *J Cardiovasc Magn Reson* 2009; **11**: 40.
38. Chen G, Jiang H, Yao Y, *et al.* Macrophage, a potential targeted therapeutic immune cell for cardiomyopathy. *Front Cell Dev Biol* 2022; **10**: 908790.
39. Quinlan JG, Hahn HS, Wong BL, *et al.* Evolution of the mdx mouse cardiomyopathy: physiological and morphological findings. *Neuromuscul Disord* 2004; **14**: 491–496.
40. Gardner RT, Habecker BA. Infarct-derived chondroitin sulfate proteoglycans prevent sympathetic reinnervation after cardiac ischemia-reperfusion injury. *J Neurosci* 2013; **33**: 7175–7183.
41. Stallcup WB, You W, Kucharova K, *et al.* NG2 proteoglycan-dependent contributions of pericytes and macrophages to brain tumor vascularization and progression. *Microcirculation* 2016; **23**: 122–133.
42. White IA, Gordon J, Balkan W, *et al.* Sympathetic reinnervation is required for mammalian cardiac regeneration. *Circ Res* 2015; **117**: 990–994.
43. Consalvi S, Mozzetta C, Bettica P, *et al.* Preclinical studies in the mdx mouse model of Duchenne muscular dystrophy with the histone deacetylase inhibitor givinostat. *Mol Med* 2013; **19**: 79–87.
44. Stallcup WB. The NG2 proteoglycan in pericyte biology. In *Pericyte Biology - Novel Concepts Advances in Experimental Medicine and Biology* (Vol. 1109), Birbrair A (ed). Springer International Publishing: Cham, 2018; 5–19.
45. Trembley MA, Velasquez LS, De Mesy Bentley KL, *et al.* Myocardium-related transcription factors control the motility of epicardium-derived cells and the maturation of coronary vessels. *Development* 2015; **142**: 21–30.
46. Quijada P, Park S, Zhao P, *et al.* Cardiac pericytes mediate the remodeling response to myocardial infarction. *J Clin Invest* 2023; **133**: e162188.

SUPPLEMENTARY MATERIAL ONLINE

Figure S1. FACS analysis of bone marrow-derived MPs from and FACSymphony gating strategy

Figure S2. Cardiac innervation in young mice

Figure S3. Cardiac fibrosis in young mice

Figure S4. Body weight, heart weight, and heart weight to tibia length ratio and evaluation of dystrophin expression

Table S1. Echocardiographic parameters

Table S2. List of primers used for mouse genes